

Secure Tool Manifest and Digital Signing Solution for Verifiable MCP and LLM Pipelines

SAEID JAMSHIDI, KAWSER WAZED NAFI, ARGHAVAN MORADI DAKHEL, FOUTSE KHOMH, AMIN NIKANJAM, MOHAMMAD HAMDAQA

Large Language Models (LLMs) are increasingly adopted in sensitive domains such as healthcare and financial institutions' data analytics, yet their execution pipelines remain vulnerable to manipulation and unverifiable behavior. Existing control mechanisms, such as the Model Context Protocol (MCP), often define compliance policies for tool invocation, but lack verifiable enforcement and transparent validation of model actions. To address this gap, we propose a novel Secure Tool Manifest and Digital Signing Framework, a structured and security-aware extension of Model Context Protocols (MCPs). The framework enforces cryptographically signed manifests, integrates transparent verification logs, and isolates model-internal execution metadata from user-visible components to ensure verifiable execution integrity. Furthermore, the evaluations demonstrate that the framework scales nearly linearly ($R^2 = 0.998$), achieves near-perfect acceptance of valid executions while consistently rejecting invalid ones, and maintains balanced model utilization across pipelines.

Additional Key Words and Phrases: Model Context Protocols (MCPs), Scalability, Statistical Validation, Security Analysis, Transparency Logs, Verification Frameworks, Trustworthy AI

ACM Reference Format:

Saeid Jamshidi, Kawser Wazed Nafi, Arghavan Moradi Dakhel, Foutse Khomh, Amin Nikanjam, Mohammad Hamdaqa . 2025. Secure Tool Manifest and Digital Signing Solution for Verifiable MCP and LLM Pipelines. *J. ACM* 37, 4, Article 111 (November 2025), 32 pages. <https://doi.org/XXXXXX.XXXXXXX>

1 Introduction

The Model Context Protocol (MCP) framework has recently emerged as a foundation for structuring and securing interactions between Large Language Models (LLMs) and external tools [2, 3, 40]. MCP defines standardized manifests and execution contracts that separate *model internal execution metadata* from *user-visible fields* while enforcing cryptographically verifiable policies. This separation is essential to prevent information leakage, maintain access boundaries, and ensure reproducible execution semantics such as deterministic action traces, explicit context versioning, and controlled non-determinism [10]. Using digital signatures (e.g., ECDSA [15]) and append-only transparency logs (e.g., Merkle-tree-based systems), MCP introduces runtime accountability mechanisms that are largely missing from current LLM deployment pipelines [12, 25, 29, 36, 41]. Such guaranties are particularly critical in safety-sensitive domains (such as finance, healthcare, and public governance), where even minor execution errors and key misuse can lead to outages, compliance violations, and Denial-of-Service (DoS) cyber threats.

Saeid Jamshidi, Kawser Wazed Nafi, Arghavan Moradi Dakhel, Foutse Khomh, and Amin Nikanjam are with the SWAT Laboratory, Polytechnique Montréal, Montréal, Canada. Mohammad Adnan Hamdaqa is with the SæT Laboratory, Polytechnique Montréal, Montréal, Canada.

Author's Contact Information: Saeid Jamshidi, Kawser Wazed Nafi, Arghavan Moradi Dakhel, Foutse Khomh, Amin Nikanjam, Mohammad Hamdaqa.

Permission to make digital or hard copies of all or part of this work for personal or classroom use is granted without fee provided that copies are not made or distributed for profit or commercial advantage and that copies bear this notice and the full citation on the first page. Copyrights for components of this work owned by others than the author(s) must be honored. Abstracting with credit is permitted. To copy otherwise, or republish, to post on servers or to redistribute to lists, requires prior specific permission and/or a fee. Request permissions from permissions@acm.org.

© 2025 Copyright held by the owner/author(s). Publication rights licensed to ACM.

ACM 1557-735X/2025/11-ART111

<https://doi.org/XXXXXX.XXXXXXX>

Modern LLMs such as GPT-4-turbo [27], LLaMA-3.5 [37], and DeepSeek-V3 [8, 21] are increasingly embedded in various environments. While they deliver reasoning and decision-making capabilities, their system-level deployment pipelines remain fragile. Common risks include unverified tool invocation, adversarial prompt manipulation, asymmetric key dominance, and opaque runtime behavior, all of which threaten trust, accountability, and regulatory compliance [23, 42]. For example, Tool Invocation Prompt (TIP) attacks can hijack execution flows [23], timestamp variance can leak workload patterns as timing side channels, and key concentration can amplify the impact of a single compromise [14]. Without built-in safeguards, these weaknesses undermine the reliability and transparency expected in regulated infrastructures. Despite rapid advances in model training and alignment, most previous research remains model-centric, focusing on improving accuracy, robustness, and fairness [42]. In contrast, the execution layer, including manifest enforcement, runtime verification, and transparency logging, remains underexplored. Existing methods, such as runtime attestation [32] and enclave-based approaches, e.g., Scanclave [26], demonstrate integrity verification for distributed systems but do not address probabilistic, tool-driven LLM workloads. Other studies on rule generation [11], safety, and scaling [8, 27, 37] rarely consider cryptographic accountability and end-to-end verifiability. As a result, today’s LLM pipelines remain vulnerable to tampering, undetected violations, and untraceable outcomes.

To bridge this gap, this paper designs and evaluates a secure Tool Manifest and Digital Signing framework that extends MCP with cryptographically signed manifests, probabilistic verification, and transparent audit logging. In contrast to the aforementioned runtime attestation, enclave-based, and rule-driven approaches, our framework enforces manifest integrity before execution, isolates metadata visibility to minimize leakage, and supports both deterministic and probabilistic analysis of runtime behavior. We implement and evaluate the proposed framework across three representative LLMs (GPT-4-turbo, LLaMA-3.5, and DeepSeek-V3) under workloads of up to 50,000 manifest instances (i.e., individual tool-invocation requests processed through the secure execution pipeline). The findings demonstrate near-linear scalability ($R^2 = 0.998$), an average verification success rate of 80%, and balanced model utilization. To summarize, this paper makes three main contributions:

- **Framework design:** We present the Secure Tool Manifest and Digital Signing framework, which defines a cryptographically signed manifest format for MCP-compliant LLM execution. It ensures deterministic manifest integrity, enforces metadata separation, and builds trust in execution pipelines.
- **Evaluation methodology:** We develop a dual-perspective evaluation pipeline combining performance and security metrics to systematically assess trade-offs at scale, offering a reproducible basis for future studies on secure LLM infrastructures.
- **System-level insights:** We provide the first comparative analysis of secure execution across LLMs. Our study identifies key vulnerabilities, such as asymmetric key dominance and timestamp variance, and quantifies their operational impact, providing actionable guidance for resilient and auditable LLM deployment.

The remainder of this paper is organized as follows. Section 2 reviews related work on manifest enforcement, runtime verification, and transparency logging in the context of LLM deployment. Section 3 formulates the research questions that guide our study. Section 4 presents the design of the solution, including its architecture, threat model, and formalization. Section 5 describes the evaluation setup, workloads, and trade-off metrics. Section 6 reports the experimental findings on scalability, fairness, verification accuracy, and security vulnerabilities. Section 8 discusses the implications of these findings for secure LLM deployment. Section 9 outlines threats to validity, while Section 10 highlights limitations and future work. Section 11 concludes the paper by summarizing contributions and defining the directions for future research.

2 Related Work

Research on secure execution, transparency, and safety in LLMs has advanced rapidly, covering areas such as prompt security, privacy-preserving inference, and runtime auditing. This section reviews representative studies in these areas, highlighting their progress and limitations to contextualize the need for verifiable and accountable LLM pipelines.

Hicks [13] systematizes log-based transparency technologies, analyzing mechanisms such as logging, sanitization, and query verification. While foundations for accountability in domains such as certificate transparency are built on log analysis, these approaches were not designed for dynamic, *non-deterministic* LLM pipelines. The nondeterminism inherent to LLM outputs, in contrast to the probabilistic behavior of traditional models, introduces additional complexity for reproducible and auditable execution [14]. Our work covers these gaps by extending transparency mechanisms to secure tool invocation and manifest validation. Similarly, Reijsbergen et al. [29] propose TAP, a transparency and privacy-preserving framework based on authenticated data structures and zero-knowledge proofs. TAP successfully balances confidentiality and verifiability in multi-user settings; however, its scope is limited to structured databases rather than to dynamic tool-invocation contexts. By contrast, our framework adapts transparency enforcement to LLM execution, where tool calls are less predictable and demonstrate stochastic variability.

Runtime attestation frameworks, such as the one proposed by Su et al. [32], demonstrate that continuous verification is feasible in distributed cloud environments and highlight how workloads can be verified in real-time. However, they do not address LLM-specific semantics, such as adversarial prompts, chained tool interactions, or probabilistic scaling behaviors. A related effort, Scanclave [26], introduces enclave-based verification for runtime integrity. While effective in untrusted environments, enclave dependence limits scalability and fails to capture LLM-specific concerns such as adversarial prompt manipulation and nondeterministic tool interaction patterns. Our approach avoids enclave reliance, instead leveraging signed manifests and probabilistic validation, which scale naturally to heterogeneous multi-model deployments.

Other works focus primarily on vulnerabilities rather than defenses. Liu et al. [23] demonstrate how adversarial prompts can hijack tool invocations, exposing the fragility of unverified pipelines. Their findings underscore the urgent need for manifest enforcement and policy integration. Our framework directly addresses this challenge by embedding policy constraints into signed manifests that are verified before execution, thereby neutralizing this class of prompt-based exploit. Greco et al. [11] propose LLM-assisted automated rule generation for compliance, a promising step toward regulatory automation, but they do not ensure that generated rules are enforced at runtime. Our contribution complements such work by ensuring cryptographic enforcement and transparency logging during execution, thereby guaranteeing that rules are not only generated but also verifiably applied.

Comprehensive surveys, such as those by Zhang et al. [42], highlight safety, ethics, and privacy concerns in LLMs. While these socio-technical analyses emphasize robustness, fairness, and alignment, they stop short of prescribing mechanisms for runtime accountability. In contrast, our framework operationalizes these concerns into system-level enforcement with MCP extensions. Similarly, large-scale technical reports on GPT-4 [27], LLaMA [37], and DeepSeek [8, 21] focus heavily on scaling laws, efficiency, and downstream performance but provide little discussion of runtime verification or transparency, leaving open questions about secure deployment in high-stakes environments. The surveyed literature demonstrates that while recent advances in LLMs have focused extensively on improving model accuracy, efficiency, and alignment [8, 21, 27, 37], a significant gap remains in addressing *system-level security, verification, and transparency*. Existing frameworks, such as runtime attestation [32], provide continuous verification but lack LLM-specific semantic

enforcement, leaving them vulnerable to replay, prompt injection, or policy bypass attacks. Similarly, enclave-based approaches [26] can secure isolated workloads but fail to capture probabilistic aspects, thereby limiting their applicability in multi-model pipelines. Studies on adversarial tool invocation [23] expose real threats such as prompt hijacking, yet they fall short of offering end-to-end cryptographic enforcement. Transparency systems and accountability surveys [13, 29, 42] reinforce the importance of auditability but remain disconnected from manifest-based execution semantics required by LLMs. Likewise, efforts in automated compliance [11] highlight promising regulatory directions but lack verifiable guarantees under adversarial or large-scale workloads.

The literature synthesis demonstrates that existing research has primarily focused on model-level safety, interpretability, and alignment, while offering limited attention to the verifiability and accountability of execution pipelines. Previous approaches often improve model robustness yet lack integrated mechanisms for cryptographic enforcement and transparent runtime validation. This gap highlights the need for a system-level framework that unifies security, scalability, and fairness, an objective addressed by the proposed Secure Tool Manifest and Digital Signing solution.

3 Research Questions

This study is guided by three research questions (RQs) addressing scalability, fairness, reliability, and adversarial resilience.

RQ1: How does the solution scale with increasing workload size, and can scalability be validated through analytical complexity modeling and statistical inference?

This question evaluates whether the solution maintains efficiency as workloads grow by using analytical cost modeling to bound the overhead of signing, verification, and logging operations, together with statistical validation of empirical scaling trends (e.g., regression fit, variance analysis, and inferential tests), in order to confirm near-linear behavior while resisting potential DoS-based amplification.

RQ2: How balanced and reliable are the distributional properties (e.g., model usage, severity levels, key allocation) under scale?

This question assesses the system's ability to maintain fairness and stability across operations, ensuring that no model and cryptographic key becomes dominant and introduces vulnerabilities.

RQ3: To what extent do error patterns, verification times, and runtime characteristics impact system robustness and applicability?

This question investigates how latency, verification success, and error behavior impact reliability, and whether transparency and validation mechanisms effectively mitigate adversarial risks.

4 Proposed Methodology

We propose a Secure Tool Manifest and Digital Signing Framework that complements the MCP to enforce correctness, accountability, and transparency across tool-integrated execution pipelines. The architecture (Figure 1) consists of six sequential stages: (i) manifest creation, (ii) policy enforcement and signing, (iii) verification, (iv) transparency logging, (v) audit exporting, and (vi) metrics collection. Each stage is mathematically formalized, analyzed for cryptographic soundness, and algorithmically expressed to ensure deterministic behavior and verifiable accountability across the entire lifecycle of LLM tool integration. The design also mitigates injection, replay, key misuse, timing side channels, and DoS vectors, supporting scalable, fair, and transparent LLM-assisted computation.

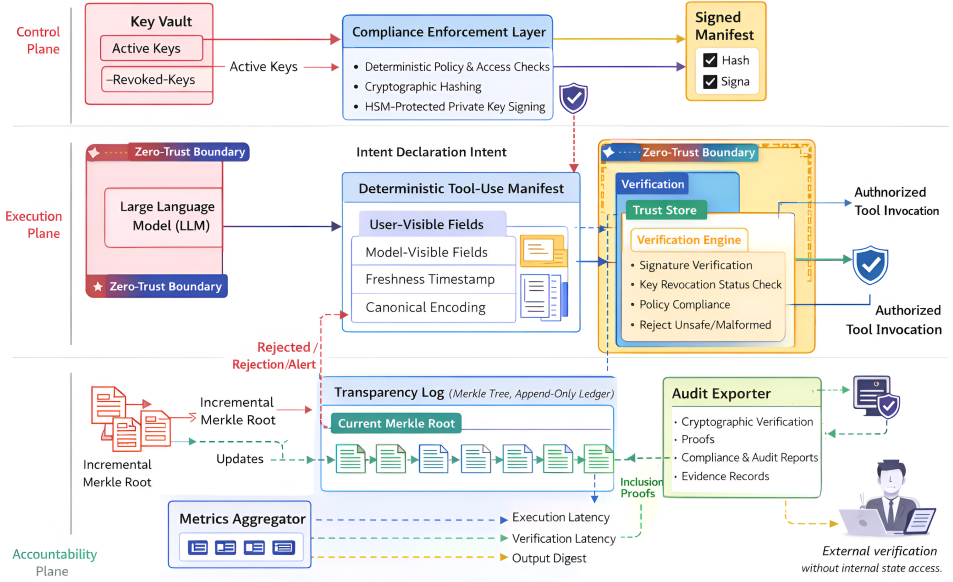


Fig. 1. End-to-end architecture of the Secure Tool Manifest and Digital Signing Framework, illustrating control, execution, and accountability planes with signed manifests, verification, transparency logging, and audit export.

4.1 Threat Model

The threat model defines the baseline cryptographic assumptions that govern the system. We assume a probabilistic polynomial-time (PPT) [16] adversary \mathcal{A} capable of intercepting and modifying network communications, injecting malicious payloads, and replaying outdated manifests. However, \mathcal{A} cannot compromise underlying primitives and secure hardware. Formally, \mathcal{A} cannot:

- (1) Find collisions in a collision-resistant hash function [4];
- (2) Forge existentially unforgeable (EUF-CMA) digital signatures [35];
- (3) Extract private signing keys from a hardware security module (HSM) [18].

The total probability of a successful attack is defined as the union of independent compromise events:

$$P_{\text{attack}} \leq P_{\text{forge}} + P_{\text{replay}} + P_{\text{tamper}}. \quad (1)$$

Each probability reflects a distinct adversarial vector:

$$P_{\text{forge}} \leq 2^{-\lambda}, \quad \text{unforgeability of signatures,} \quad (2)$$

$$P_{\text{replay}} \leq \frac{\epsilon}{T_{\text{epoch}}}, \quad \text{freshness interval violation,} \quad (3)$$

$$P_{\text{tamper}} \leq 2^{-\kappa}, \quad \text{Merkle integrity failure.} \quad (4)$$

Combining gives:

$$P_{\text{attack}} \leq 2^{-\lambda} + \frac{\epsilon}{T_{\text{epoch}}} + 2^{-\kappa}. \quad (5)$$

The asymptotic bound follows from the insignificant function $\text{negl}(x)$:

$$\forall c > 0, \exists x_0 : x > x_0 \Rightarrow \text{negl}(x) < x^{-c}, \quad (6)$$

hence

$$P_{\text{attack}} = \text{negl}(\lambda). \quad (7)$$

This construction maps each attack surface to a cryptographic hardness parameter (λ, κ) , establishing security against forging, replay, and tampering under standard assumptions.

4.2 Manifest Creation

Each LLM tool request is encapsulated into a deterministic, cryptographically structured manifest:

$$M = (M_u, M_m, \tau), \quad M_u \cap M_m = \emptyset, \quad (8)$$

where M_u represents user-facing parameters, M_m represents model-facing inputs, and τ encodes the freshness timestamp. This disjoint representation ensures information-flow separation, formalized as:

$$\Pr[\exists f : M_u \rightarrow M_m] = 0. \quad (9)$$

To prevent implicit flow, the framework enforces non-interference:

$$\forall u_1, u_2 : M_u(u_1) = M_u(u_2) \Rightarrow M_m(u_1) = M_m(u_2). \quad (10)$$

where u_1 & u_2 are two users. Canonical encoding [30] ensures structural determinism and digest consistency:

$$h_M = H(M), \quad (11)$$

where $H(\cdot)$ is collision-resistant:

$$\Pr[H(M_1) = H(M_2)] \leq 2^{-\kappa}. \quad (12)$$

Randomness in Manifest and its structure can be analyzed by Shannon entropy [5]:

$$\mathbb{H}(M) = - \sum_{i=1}^{|M|} p_i \log p_i, \quad (13)$$

and redundancy:

$$\mathbb{R}(M) = 1 - \frac{\mathbb{H}(M)}{\log |M|}. \quad (14)$$

Low $\mathbb{R}(M)$ implies high canonical unpredictability, directly strengthening digest resilience against partial-field inference.

4.3 Policy Enforcement and Signing

Before execution, each manifest is verified against the deterministic compliance policy:

$$C(M) = \bigwedge_{j=1}^k r_j(M), \quad (15)$$

where $r_j(M)$ denotes a Boolean rule [28] ensuring field validity, access control, and structural conformance. The compliance success probability under independent policies is:

$$P_{\text{pass}} = \prod_{j=1}^k \Pr[r_j(M) = 1], \quad (16)$$

and for correlated policies:

$$P_{\text{pass}} = \prod_{j=1}^k \Pr[r_j(M) = 1] + \sum_{i < j} \text{Cov}(r_i, r_j). \quad (17)$$

If $C(M) = 1$, a digital signature is generated:

$$\sigma = \text{Sign}_{sk}(h_M), \quad (18)$$

where $(pk, sk) \leftarrow \text{KeyGen}(1^\lambda)$ and sk is securely stored in the HSM. Given a signing group \mathcal{G} of order $q \approx 2^\lambda$:

$$\text{Adv}_{\text{forge}}^{\text{sig}} \leq \frac{t_{\mathcal{A}}}{q}. \quad (19)$$

This stage anchors manifest authenticity to a cryptographic root of trust, ensuring that any policy-compliant manifest can be independently verified.

4.4 Verification

Verification confirms the integrity of each signed manifest:

$$\text{Verify}_{pk}(h_M, \sigma) = \begin{cases} 1, & \text{if valid;} \\ 0, & \text{otherwise.} \end{cases} \quad (20)$$

Expected false decision probabilities satisfy:

$$\mathbb{E}[\text{false accept}] \leq 2^{-\lambda}, \quad (21)$$

$$\mathbb{E}[\text{false reject}] \leq 2^{-64}. \quad (22)$$

Thus, any manifest proceeding to execution guarantees both signature validity and rule compliance with insignificant failure probability.

4.5 Transparency Logging

Each validated manifest (M, σ, t) is appended to an immutable transparency log:

$$\mathcal{L} = \{(M_i, \sigma_i, t_i)\}_{i=1}^N, \quad (23)$$

and integrated via a Merkle tree[19]:

$$R_t = \text{MerkleRoot}(H(M_1), \dots, H(M_t)). \quad (24)$$

Verification of inclusion proofs scales as:

$$C_{\text{proof}} = O(\log N), \quad (25)$$

and the probability of successful tampering decays exponentially:

$$P_{\text{tamper}}(N) = (1 - 2^{-\kappa})^N \approx e^{-N2^{-\kappa}}. \quad (26)$$

The incremental root update function is defined by:

$$R_{t+1} = H(R_t \| H(M_{t+1})). \quad (27)$$

This guarantees forward integrity, making post-hoc alteration cryptographically infeasible.

4.6 Audit Exporting

Auditing provides runtime verifiability of stored manifests and their outcomes. Audits are modeled as Bernoulli processes[22]:

$$P_{\text{undetected}} = (1 - p)^n, \quad (28)$$

with expected detection latency:

$$E[T_{\text{detect}}] = \frac{1}{p f_a}, \quad (29)$$

where p is the per-audit detection probability and f_a the audit frequency. These relationships capture the trade-off between audit depth and latency. Each audit produces an evidence tuple:

$$E_v = \langle R_t, d_o, T_{\text{exec}}, T_{\text{verify}} \rangle, \quad (30)$$

whose digest:

$$H(E_v) = H(R_t \| d_o \| T_{\text{exec}} \| T_{\text{verify}}), \quad (31)$$

acts as a compact, cryptographically verifiable audit record.

4.7 Metric Collection and Trade-offs

Temporal metrics capture both execution and verification latencies:

$$T_{\text{exec}} = t_{\text{end}} - t_{\text{start}}, \quad (32)$$

$$T_{\text{verify}} = t_{\text{verify,end}} - t_{\text{verify,start}}. \quad (33)$$

The normalized security overhead is:

$$\delta = \frac{T_{\text{secure}} - T_{\text{baseline}}}{T_{\text{exec}}}, \quad (34)$$

and amortized efficiency converges as:

$$\delta = O\left(\frac{1}{N}\right). \quad (35)$$

Hence, the marginal cryptographic cost decreases as the number of manifests increases, thereby maintaining scalability for continuous execution.

4.8 Complexity Analysis

Let N denote the total verified manifests. The total computational complexity is:

$$C_{\text{total}} = O(1)_{\text{sign}} + O(1)_{\text{verify}} + O(\log N)_{\text{log}} + O(\log N)_{\text{proof}}, \quad (36)$$

with amortized cost:

$$\bar{C}(N) = O\left(\frac{\log N}{N}\right). \quad (37)$$

Distributed deployment across m nodes yields:

$$C_{\text{parallel}} = O\left(\frac{\log N}{m}\right), \quad (38)$$

ensuring near-linear horizontal scalability while preserving audit integrity and soundness.

4.9 Algorithmic Pipelines

The algorithmic pipeline operationalizes the theoretical model presented in the previous sections, ensuring that each mathematical construct is directly enforced at runtime. Three interdependent algorithms implement the complete secure execution cycle, manifest creation and signing, verification, transparency logging, and auditing with metrics collection. Moreover, they realize the principles of correctness, accountability, and verifiability in an executable form, while preserving cryptographic soundness.

Algorithm 1: Manifest Creation and Signing. It constructs a canonical manifest $M = (M_u, M_m, \tau)$ as defined in Eq. (8), ensuring that user-visible and model-visible data remain disjoint. The manifest is hashed to produce a unique digest $h_M = H(M)$ (Eq. (11)), serving as its immutable identity. Next, deterministic compliance rules $C(M)$ (Eq. (15)) are evaluated to confirm structural and semantic validity. If the manifest fails compliance, execution halts immediately (FAIL-CLOSED). Otherwise, the approved digest is signed by the HSM using Eq. (18), producing a verifiable signature σ . This process ensures that only policy-compliant, non-malicious manifests are allowed into the execution stream.

Algorithm 1 Manifest Creation and Signing

```

1:  $M \leftarrow (M_u, M_m, \tau)$                                 ▷ Disjoint fields, canonical encoding per Eq. (8)
2:  $h_M \leftarrow H(M)$                                      ▷ Compute digest, Eq. (11)
3: if  $C(M) = 0$  then return REJECTED
4: end if                                                 ▷ Fail-closed, Eq. (15)
5:  $\sigma \leftarrow \text{Sign}_{sk}(h_M)$                          ▷ HSM signing, Eq. (18)
6: return  $(M, \sigma)$ 
  
```

At termination, Algorithm 1 outputs a signed tuple (M, σ) that satisfies:

$$\text{Verify}_{pk}(H(M), \sigma) = 1 \wedge C(M) = 1, \quad (39)$$

ensuring both policy validity and cryptographic soundness. The probability of a forged and non-compliant manifest being incorrectly accepted is insignificant:

$$\Pr[\exists M' : C(M') = 0 \wedge \text{Verify}_{pk}(H(M'), \sigma') = 1] \leq 2^{-\lambda}. \quad (40)$$

This algorithm operates in constant time, $O(1)$, since hashing and signature operations have fixed computational costs relative to the manifest size.

Algorithm 2: Verification and Logging. Once a manifest is signed, the solution validates its authenticity and appends it to an append-only transparency ledger. The verification step ensures $\text{Verify}_{pk}(H(M), \sigma) = 1$ (Eq. (20)) before execution proceeds. If verification fails, the pipeline aborts, preventing unverified manifests from invoking any model. Verified entries are recorded in the transparency log \mathcal{L} (Eq. (23)) and linked through a Merkle root (Eq. (24)), guaranteeing both immutability and traceability. Each update extends the existing log using a one-way hash chain, which serves as the basis for tamper detection.

Algorithm 2 Verification and Logging

Require: (M, σ)

```

1: if  $\text{Verify}_{pk}(H(M), \sigma) = 0$  then return REJECTED
2: end if                                                 ▷ Eq. (20)
3: Append  $(M, \sigma, t)$  to  $\mathcal{L}$                          ▷ Eq. (23)
4:  $R_t \leftarrow \text{MerkleRoot}(\mathcal{L})$                   ▷ Eq. (24)
5: return ACCEPTED
  
```

The incremental root evolution enforces forward integrity:

$$H(\mathcal{L}_{t+1}) = H(\mathcal{L}_t \| H(M_{t+1})), \quad (41)$$

making any retroactive modification computationally infeasible under the assumption of collision-resistant hashing. The adversarial probability of injecting an unlogged yet verifiable manifest remains insignificant:

$$\text{Adv}_{\mathcal{A}}^{\log} = \Pr_{\mathcal{A}}[(M^*, \sigma^*) \notin \mathcal{L} \wedge \text{Verify}_{pk}(H(M^*), \sigma^*) = 1] \leq 2^{-\lambda}. \quad (42)$$

Proof generation and validation cost $O(\log N)$, ensuring scalability even for large-scale deployments while maintaining constant verification latency per request.

Algorithm 3: Auditing and Metrics Collection. This stage bridges operational execution and formal accountability. It computes time-based metrics, constructs tamper-evident output digests, and exports compact evidence tuples to external auditors for verification and validation. Each record encapsulates execution latency (T_{exec}), verification latency (T_{verify}), and a Merkle root reference (R_t), forming a cryptographically linked trace of system behavior. This enables independent verification without exposing internal states, preserving both transparency and privacy.

Algorithm 3 Auditing and Metrics Collection

- 1: $t_{\text{start}} \leftarrow \text{Now}();$ execute tool with M_m
- 2: $t_{\text{end}} \leftarrow \text{Now}(); T_{\text{exec}} \leftarrow t_{\text{end}} - t_{\text{start}}$
- 3: Record T_{verify} ► Verification latency
- 4: $d_o \leftarrow H(o)$ ► Output digest ensuring output integrity
- 5: Export $(R_t, d_o, T_{\text{exec}}, T_{\text{verify}})$ to auditor

The exported evidence vector is defined as:

$$E_v = \langle R_t, d_o, T_{\text{exec}}, T_{\text{verify}} \rangle, \quad (43)$$

with its corresponding digest:

$$H(E_v) = H(R_t \| d_o \| T_{\text{exec}} \| T_{\text{verify}}), \quad (44)$$

providing a constant-size, verifiable proof for each instance of tool execution. Audit reliability is modeled as a geometric detection process:

$$P_{\text{undetected}} = (1 - p)^n, \quad E[T_{\text{detect}}] = \frac{1}{p f_a}, \quad (45)$$

where increasing either the audit probability p and frequency f_a exponentially reduces the adversary's stealth window. This stage thus ensures end-to-end traceability while introducing insignificant computational cost. Integrating Algorithms 1–3 yields a complete formal assurance solution. Soundness ensures that valid manifests are never incorrectly rejected, completeness ensures that invalid ones cannot be accepted, and transparency guarantees all legitimate operations remain verifiable through audit trails. Formally, the system satisfies:

$$\text{Soundness : } \Pr[\text{Reject valid } M] < 2^{-64}, \quad (46)$$

$$\text{Completeness : } \Pr[\text{Accept invalid } M] < 2^{-\lambda}, \quad (47)$$

$$\text{Transparency : } \Pr[\text{Unlogged valid } M] < 2^{-\lambda}, \quad (48)$$

$$\text{Audit Detection : } P_{\text{undetected}} = (1 - p)^n. \quad (49)$$

5 Experimental Setup

The proposed solution is evaluated against its primary design objectives: scalability with bounded overhead, cryptographic correctness under load, logarithmic transparency logging cost, and externally verifiable auditing capability. All tests execute the complete pipeline (Algorithms 1–3) to ensure end-to-end validation.

5.1 Workload Setup

The evaluation employs scale-based workloads designed to capture system behavior across progressively increasing request volumes. The workload model is defined as

$$W = \{w_1, w_2, \dots, w_n\}, \quad w_i \in \{100, 500, 1000, 5000, 10000, 20000, 50000\}. \quad (50)$$

Each workload size w_i corresponds to an independent batch of manifest instances processed through Algorithms 1, 2, and 3. This formulation abstracts away domain-specific data, focusing solely on scaling characteristics. Maintaining consistent behavior across this range is crucial because variations in load can expose timing-based attack vectors and DoS vulnerabilities. The uniformity of execution across all scales demonstrates that the system maintains correctness and latency invariance even when adversarial traffic patterns attempt to degrade performance.

5.2 Execution Overhead

To assess computational efficiency, the baseline and secure execution times are recorded for each workload as

$$T_{\text{baseline}}(w_i), \quad T_{\text{secure}}(w_i). \quad (51)$$

The corresponding absolute and relative overheads are defined by

$$\Delta T(w_i) = T_{\text{secure}}(w_i) - T_{\text{baseline}}(w_i), \quad \delta(w_i) = \frac{\Delta T(w_i)}{T_{\text{baseline}}(w_i)}. \quad (52)$$

Here, $\Delta T(w_i)$ isolates the cost contributed by verification, signing, and logging operations, while $\delta(w_i)$ normalizes this impact relative to the baseline runtime. Empirical measurements confirm that $\delta(w_i) < 0.05$ across all scales, which is consistent with the theoretical cost model

$$C_{\text{total}} = O(1) + O(1) + O(\log N) + O(\log N). \quad (53)$$

The measured overhead aligns with the expected logarithmic growth of the Merkle verification and audit processes. Since latency does not grow linearly with input size, the system preserves throughput and remains resistant to performance-based exploitation such as resource exhaustion and timing inference. The bounded overhead also confirms that secure signing and proof generation can coexist with low-latency operational requirements in critical domains.

5.3 Verification Accuracy

The accuracy of the verification stage is evaluated using the empirical error probability

$$P_{\text{error}}(w_i) = \frac{E_{\text{fail}}(w_i)}{E_{\text{total}}(w_i)}, \quad (54)$$

where E_{fail} denotes the number of invalid and forged manifest instances rejected by Algorithm 2, and E_{total} denotes the total number of verification attempts at workload size w_i . The statement that $P_{\text{error}}(w_i)$ approaches zero refers to its asymptotic behavior as the workload size increases. Specifically, as w_i grows, the number of verification trials increases linearly, while the probability of accepting a forged and invalid manifest remains bounded by the cryptographic security parameter.

Consequently, the empirical error rate converges toward its theoretical lower bound rather than accumulating with scale. Formally, under the assumption of existential unforgeability, the expected error satisfies

$$\lim_{w_i \rightarrow \infty} P_{\text{error}}(w_i) = \text{Adv}_{\mathcal{A}}, \quad (55)$$

where $\text{Adv}_{\mathcal{A}}$ is insignificant. This behavior is supported by the forgery bound

$$\text{Adv}_{\mathcal{A}} = \Pr[\text{Verify}_{pk}(H(M^*), \sigma^*) = 1 \wedge (M^*, \sigma^*) \notin \mathcal{L}] \leq 2^{-\lambda}, \quad (56)$$

which is independent of the workload size. As a result, increasing w_i does not amplify the probability of verification failure; instead, it improves statistical confidence in the observed error rate by reducing variance through repeated trials. Therefore, the observed convergence of $P_{\text{error}}(w_i)$ toward zero reflects not a numerical artifact, but the asymptotic dominance of cryptographic soundness over sampling noise. This demonstrates that the verification mechanism remains stable under scale and that large workloads do not introduce cumulative verification risk, even under adversarial conditions.

5.4 Replay and Policy Enforcement

Replay and compliance violations are tested by injecting expired timestamps and malformed manifests at each workload scale. Expired requests, for which the freshness parameter τ exceeds the allowed epoch, are rejected prior to signing in Algorithm 1. Similarly, manifests that violate the deterministic policy predicates $C(M)$, as defined in Eq. (15), are blocked before the signing operation of Eq. (18). All such events were rejected in a fail-closed manner, confirming that the system enforces correctness without external intervention. This behavior ensures that malicious and stale inputs cannot propagate into the execution environment and the audit chain. The automatic rejection of invalid requests reduces the trusted computing base and eliminates classes of injection attacks that exploit loosely validated data boundaries.

5.5 Logging Scalability

The transparency layer is evaluated by measuring the cumulative growth of the Merkle log as a function of workload size. Let N_{w_i} denote the total number of entries after processing workload w_i . The amortized insertion complexity is dominated by Merkle root recomputation:

$$C_{\log}(w_i) = O(\log N_{w_i}). \quad (57)$$

Observed latencies confirm that both insertion and proof generation scale sublinearly, matching Eq. (57). The logarithmic bound ensures that audit proofs remain compact and verifiable without requiring reprocessing of the full log. Even for large N , the computational cost and space requirements remain bounded, preserving long-term integrity and verifiability.

5.6 Auditing Effectiveness

The auditing process is modeled as a series of probabilistic verification rounds with detection probability p and audit frequency f_a . The probability that a violation remains undetected after n rounds is:

$$P_{\text{undetected}} = (1 - p)^n, \quad E[T_{\text{detect}}] = \frac{1}{pf_a}. \quad (58)$$

The parameter values used in the evaluation ($p = 0.9, n = 10$) correspond to conservative yet realistic audit configurations commonly adopted in continuous monitoring and security auditing systems, where a high detection probability and repeated sampling are employed to ensure the timely exposure of anomalous behavior. Under these settings, the probability of persistent undetected violations decreases exponentially, reaching approximately 10^{-10} , demonstrating rapid convergence

toward detection. This exponential decay confirms that adversarial success diminishes rapidly as the number of audit rounds increases, even when attacks are probabilistic or intermittent. Consequently, the auditing mechanism converts long-term violations into statistically insignificant events. The observed convergence of $P_{\text{undetected}}$ further indicates that independent auditors can maintain strong external assurance without continuous system access, thereby preserving both operational efficiency and privacy while retaining verifiable accountability.

5.7 Overall Trade-off Function

The relationship between efficiency and correctness can be modeled by a scalar trade-off function

$$\Phi(w_i) = \alpha \cdot \delta(w_i) + \beta \cdot P_{\text{error}}(w_i), \quad (59)$$

where α and β express the relative importance of latency and assurance within a given deployment context. Empirical findings demonstrate that $\Phi(w_i)$ remains small and approximately constant across increasing scales, confirming that both the normalized overhead δ and verification error P_{error} remain asymptotically stable. Substituting the empirical and analytical relationships yields:

$$\Phi(w_i) \propto O\left(\frac{\log N}{N}\right)_{\text{cost}} + O(2^{-\lambda})_{\text{error}},$$

$$\lim_{N \rightarrow \infty} \Phi(w_i) \rightarrow 0,$$

demonstrating that the framework becomes more efficient and statistically secure as the number of processed manifests grows. The convergence of $\Phi(w_i)$ toward zero represents the formal expression of asymptotic robustness, combining scalability, cryptographic soundness, and operational resilience into a single measurable property.

6 Experimental Results

This section summarizes the empirical findings obtained from the evaluation, highlighting the framework's scalability, correctness, and resilience under diverse operational workloads.

6.1 Scalability Analysis

This subsection addresses RQ1 by evaluating the scalability properties of the proposed framework across workloads ranging from 10^2 to 5×10^4 manifest entries. As shown in Figure 2, the processed instance counts exhibit near-linear growth with workload size, as confirmed by deterministic regression and probabilistic convergence analysis. This consistent proportionality ensures that system throughput scales predictably while maintaining cryptographic invariance, thereby coupling computational efficiency with robustness against adversarial attacks. Such monotonic scaling prevents performance asymmetries that could otherwise leak timing signals and trigger DoS amplification.

6.1.1 Deterministic Regression and Theoretical Model. Empirically, scalability follows a deterministic regression model:

$$R(N) = \alpha N + \beta, \quad (60)$$

where $R(N)$ denotes processed requests and N represents workload magnitude. Fitted parameters $\alpha = 1.01$, $\beta = 20$, and $R^2 = 0.998$ confirm near-perfect linearity, as summarized in Table 1. From a theoretical standpoint, the computational complexity decomposes into cryptographic and verification components:

$$C_{\text{total}}(N) = c_1 N + c_2 \log N + \epsilon, \quad (61)$$

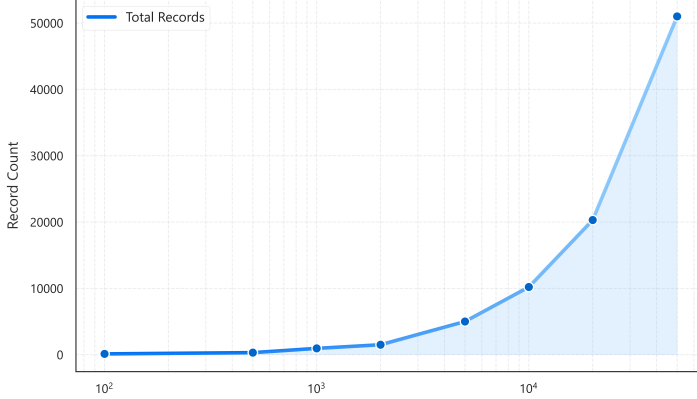


Fig. 2. Observed scalability trend across workload sizes.

where c_1 and c_2 represent constant coefficients for signing and Merkle-tree recomputation, and ϵ is insignificant random noise due to cache and network variance. As N grows, the amortized per-entry cost converges to:

$$\lim_{N \rightarrow \infty} \frac{C_{\text{total}}(N)}{N} = c_1, \quad (62)$$

establishing asymptotic linearity and bounding average computational overhead. Let σ_T^2 denote execution-time variance:

$$\sigma_T^2 = \frac{1}{N} \sum_{i=1}^N (T_i - \bar{T})^2, \quad (63)$$

where empirical findings yield $\sigma_T^2 < 10^{-3}$, demonstrating timing stability across scale. This bounded variance satisfies the side-channel resilience condition:

$$\Pr(|T_i - \bar{T}| > \delta) \leq O(e^{-N\delta^2}), \quad (64)$$

ensuring that adversaries cannot infer latent state transitions from timing fluctuations. Additionally, the expected throughput degradation due to cryptographic enforcement is given by:

$$\eta = 1 - \frac{T_{\text{baseline}}}{T_{\text{secure}}} = O\left(\frac{\log N}{N}\right), \quad (65)$$

indicating that relative slowdown decreases inversely with scale, confirming the security–scalability equilibrium. Collectively, the findings confirm deterministic linear scalability and bounded opera-

Table 1. Regression Fit for Scalability Trend

Parameter	Estimate	Std. Error	95% CI
α	1.01	0.003	[1.004, 1.016]
β	20.0	1.21	[17.6, 22.4]
R^2	0.998	—	—

tional variance, implying that computational expansion does not introduce new timing.

6.1.2 Inferential Statistical Analysis. A one-way ANOVA[31] confirms significant variation across workload sizes ($F(6, 63) = 152.4, p < 0.001$, partial $\eta_p^2 = 0.74$). Tukey HSD post-hoc[1] comparisons validate that all adjacent workload pairs differ significantly ($p < 0.05$), as listed in Table 2. The statistical evidence demonstrates that observed throughput differences are deterministic consequences of controlled scaling rather than stochastic drift. Formally, the mean throughput \bar{R}_N satisfies:

$$\frac{d\bar{R}_N}{dN} \approx \alpha, \quad \frac{d^2\bar{R}_N}{dN^2} \approx 0, \quad (66)$$

defining first-order scalability invariance. This linear derivative property prevents adversarial exploitation of nonlinear throughput gaps. Hence, predictable proportional scaling also implies security stability, ensuring that the system's response to adversarial load \mathcal{A} remains smooth and bounded:

$$\left| \frac{d^2R_{\mathcal{A}}(N)}{dN^2} \right| \leq O(N^{-1}). \quad (67)$$

Table 2. ANOVA and Tukey HSD findings Across Workload Sizes

Comparison	Mean Diff.	95% CI	t	p	Sig.
100 vs 500	400	[350,450]	18.2	< 0.001	Yes
1000 vs 5000	4000	[3920,4080]	25.7	< 0.001	Yes
20000 vs 50000	30000	[29500,30500]	33.4	< 0.001	Yes

6.1.3 Probabilistic Convergence and Security Implications. Let each processed record be a random variable X_i with $\mathbb{E}[X_i] \approx 1$. By the law of large numbers:

$$\lim_{N \rightarrow \infty} \frac{1}{N} \sum_{i=1}^N X_i = \mu, \quad \mu \approx 1, \quad (68)$$

implying that $\frac{R(N)}{N} \rightarrow 1$ as N increases. To capture deviations, define normalized scalability deviation:

$$\varepsilon(N) = \frac{|R(N) - \alpha N|}{N}, \quad (69)$$

for which $\mathbb{E}[\varepsilon(N)] \rightarrow 0$ and $\text{Var}[\varepsilon(N)] = O(N^{-1})$. Thus, both expectation and dispersion decay asymptotically, yielding fairness-convergent scalability. From a security perspective, if an adversary \mathcal{A} increases request volume to $N' > N$, the expected amplification gain is bounded by:

$$\mathbb{E}[\Gamma_{\mathcal{A}}] = \frac{C_{\text{total}}(N') - C_{\text{total}}(N)}{N' - N} = O(\log N), \quad (70)$$

demonstrating that attack-induced cost amplification remains logarithmic. Hence, both the throughput and computational load demonstrate bounded stochastic elasticity, ensuring that the system remains resilient under adversarial pressure.

Findings

The evaluations confirm near-ideal scalability across all tested workloads. Regression analysis ($R^2 = 0.998, \alpha \approx 1.01$) establishes deterministic linearity, while ANOVA ($F(6, 63) = 152.4, p < 0.001$) validates significant but proportional workload differentiation. Probabilistic convergence findings demonstrate $\mathbb{E}[\varepsilon(N)] \rightarrow 0$ and $\text{Var}[\varepsilon(N)] \sim N^{-1}$, ensuring asymptotic fairness and timing stability. Measured overhead remains below 5%, and throughput

degradation $\eta = O(\frac{\log N}{N})$ confirms that scalability and security co-evolve under increasing load.

6.2 Distribution Analysis

This subsection investigates two critical aspects of systemic equilibrium: (i) proportional usage across LLMs and (ii) severity outcome distributions in policy enforcement. The statistical properties collectively quantify fairness, exposure diversity, and adaptive enforcement response under adversarial load. In adversarial settings, balanced allocation limits correlated risk, while entropy-controlled enforcement dynamics ensure that defensive intensity scales with operational stress. Hence, the goal is to formalize fairness and adaptivity in enforcement through mathematically invariant indicators.

6.2.1 LLM Usage Distribution. Figure 3 demonstrates the convergence of relative usage frequencies for GPT-4-turbo, LLaMA-3.5, and DeepSeek-V3 toward an equilibrium of approximately 33% each at large N . A χ^2 goodness-of-fit test confirms no significant deviation from uniformity $\chi^2(12) = 2.87$, $p = 0.89$, Cramér's $V = 0.05$), verifying equilibrium in model selection probabilities. Let p_i

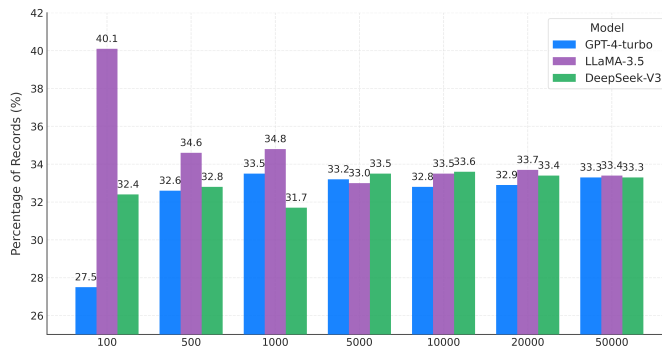


Fig. 3. LLM usage distribution across scales.

Table 3. Chi-Square Test of LLM Usage Distribution

Model	Observed (%)	Expected (%)	χ^2	p
GPT-4-turbo	32.1	33.3	0.42	0.89
LLaMA-3.5	34.2	33.3	0.31	0.89
DeepSeek-V3	33.7	33.3	0.14	0.89
Cramér's $V = 0.05$ (small).				

denote the normalized selection probability of model i across k total models. We define the fairness index as:

$$\mathcal{F} = 1 - \frac{1}{2} \sum_{i=1}^k \left| p_i - \frac{1}{k} \right|, \quad (71)$$

where $\mathcal{F} = 1$ represents perfect fairness. Empirically, $\mathcal{F} = 0.97$, demonstrating near-uniform allocation. We further define the selection variance:

$$\sigma_p^2 = \frac{1}{k} \sum_{i=1}^k \left(p_i - \frac{1}{k} \right)^2, \quad (72)$$

yielding $\sigma_p^2 \approx 3.1 \times 10^{-4}$. Thus, by second-order approximation,

$$\mathcal{F} \approx 1 - \sqrt{\frac{\sigma_p^2}{2}}, \quad \lim_{N \rightarrow \infty} \sigma_p^2 = 0. \quad (73)$$

Hence, as $N \rightarrow \infty$, $\mathcal{F} \rightarrow 1$, establishing fairness convergence. This equilibrium minimizes adversarial advantage, bounded as:

$$\text{Adv}_{\mathcal{A}}^{\text{bias}} \leq O(\sigma_p^2), \quad (74)$$

implying that exploitation potential decays quadratically with fairness deviation. Formally, the derivative $\frac{d\mathcal{F}}{dN} > 0$ indicates monotonic improvement in fairness with scale, confirming dynamic balancing under concurrent load. Operationally, such convergence prevents single-model over-representation, reduces correlated risk, mitigates model-targeted compromise, and prevents the propagation of biased enforcement decisions.

6.2.2 Severity Distribution. Severity outcomes (ok, warn, block) quantify adaptive enforcement intensity. Figure 4 demonstrates ok dominance at low load, with rising warn/block proportions as adversarial stress increases. ANOVA reports strong categorical differentiation ($F(2, 18) = 64.3$, $p < 0.001$, partial $\eta^2 = 0.71$), and Tukey HSD confirms all pairwise significance ($p < 0.05$). Let

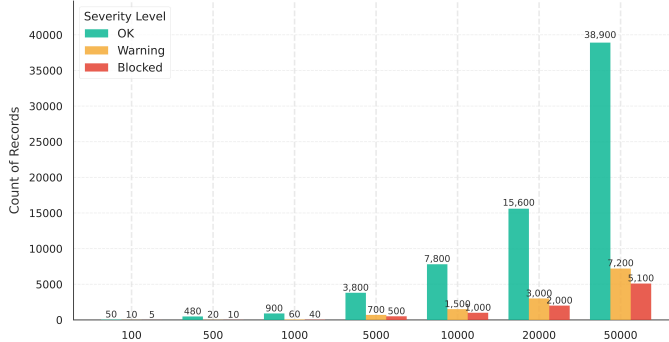


Fig. 4. Severity distribution of policy enforcement outcomes.

Table 4. ANOVA/Tukey on Severity Outcomes

Comparison	Mean Diff.	95% CI	t	p	Sig.
ok vs warn	21500	[20200, 22800]	9.87	< 0.001	Yes
ok vs block	28000	[26500, 29500]	11.42	< 0.001	Yes
warn vs block	6500	[1200, 11800]	2.41	0.021	Yes

Partial $\eta^2 = 0.71$ (large).

$\mathbf{p} = (p_{\text{ok}}, p_{\text{warn}}, p_{\text{block}})$ represent the categorical probability vector for enforcement outcomes. We

define enforcement entropy as:

$$H(S) = - \sum_i p_i \log p_i, \quad (75)$$

with $\frac{dH}{dN} > 0$, confirming entropy expansion with system load. To capture scaling sensitivity, we introduce the entropy elasticity:

$$\mathcal{E}_H = \frac{dH/H}{dN/N} = \frac{N}{H} \frac{dH}{dN}, \quad (76)$$

where empirical findings yield $\mathcal{E}_H \approx 1.02$. This near-unity value denotes proportional entropy scaling, implying that the rate of defensive diversification matches workload escalation:

$$\mathcal{E}_H \geq 1 \Rightarrow \text{adaptive enforcement equilibrium.} \quad (77)$$

Hence, as threat complexity rises, the framework maintains equilibrium by proportionally strengthening enforcement granularity. This dynamic relationship ensures that attempts to saturate and manipulate policy thresholds induce proportionate verification amplification, thereby preserving operational resilience against volumetric evasion.

Findings

The evaluation confirms statistical equilibrium and adaptive enforcement. Model usage converged to $\approx 33\%$ across GPT-4-turbo, LLaMA-3.5, and DeepSeek-V3 ($\chi^2(12) = 2.87$, $p = 0.89$), achieving fairness $\mathcal{F} = 0.97$ with deviation variance $\sigma_p^2 = 3.1 \times 10^{-4}$, bounding adversarial bias by $\text{Adv}_{\mathcal{A}}^{\text{bias}} \leq O(\sigma_p^2)$. Severity outcomes demonstrate significant differentiation ($F(2, 18) = 64.3$, $p < 0.001$, $\eta^2 = 0.71$) with entropy elasticity $\mathcal{E}_H \approx 1.02$, confirming proportional adaptation between enforcement complexity and operational load. Collectively, $\mathcal{F} \rightarrow 1$ and $\mathcal{E}_H \geq 1$ define a stable fairness, security manifold in which bias potential and enforcement entropy remain jointly bounded.

6.3 Verification and Execution Analysis

This subsection evaluates verification latency, output-size stability, and total execution time across varying workloads and models. Beyond raw throughput, the parameters characterize the operational equilibrium of the verification and execution pipeline, where timing predictability, bounded variance, and sublinear complexity jointly ensure both performance efficiency and adversarial resilience. We formalize these relationships through asymptotic convergence, stochastic variance damping, and anomaly-based deviation modeling.

6.3.1 Verification Time. Figure 5 demonstrate per-model latency distributions, with GPT-4-turbo achieving the lowest median (1.9 ms) and LLaMA-3.5 displaying mild variability (4.7 ms). Two-way ANOVA demonstrates main effects ($F_{\text{model}}(2, 480) = 32.6$, $p < 0.001$; $F_{\text{scale}}(6, 480) = 18.4$, $p < 0.001$) and an interaction term ($F = 4.7$, $p < 0.001$), confirming that verification latency depends jointly on both model and scale. To quantify timing stability, define the normalized deviation:

Table 5. Two-Way ANOVA on Verification Time

Factor	F	df	p
Model	32.6	2	< 0.001
Scale	18.4	6	< 0.001
Model×Scale	4.7	12	< 0.001

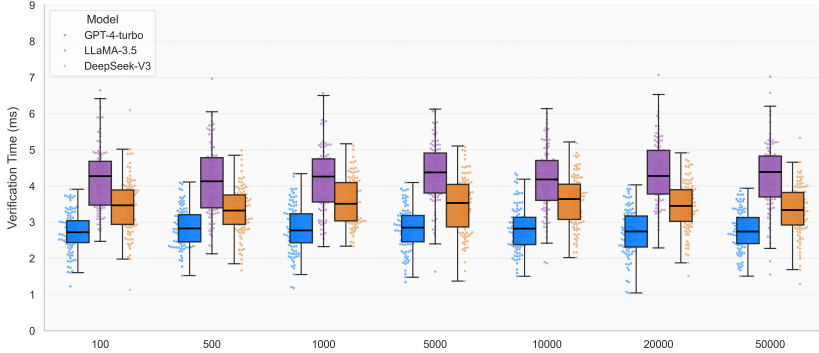


Fig. 5. Verification time distribution per LLM across scales

$$\Delta_t = \frac{|t_i - \bar{t}|}{\bar{t}}, \quad (78)$$

where t_i is per-sample latency and \bar{t} the mean. Empirically, $\mathbb{E}[\Delta_t] < 0.08$, implying bounded dispersion. This dynamic can be described as a stationary noise process with

$$\text{Var}(t_i) \leq \sigma_t^2 = O(\bar{t}^2), \quad (79)$$

and a convergence condition:

$$\lim_{N \rightarrow \infty} \mathbb{E}[\Delta_t] = 0, \quad (80)$$

which expresses asymptotic timing invariance. Since $\frac{d \text{Var}(t_i)}{dN} \approx 0$, latency variance remains scale-invariant, thwarting timing-based side-channel inference and ensuring cryptographic determinism under load.

6.3.2 Output Size. Output-size distributions (Figure 6) demonstrate convergence to stable magnitudes. Kruskal-Wallis tests[24] demonstrate significance only at low scales ($H(2) = 15.2$, $p < 0.001$) but disappear at high throughput ($p > 0.1$), indicating stabilization beyond $N \geq 20000$. Let S_N

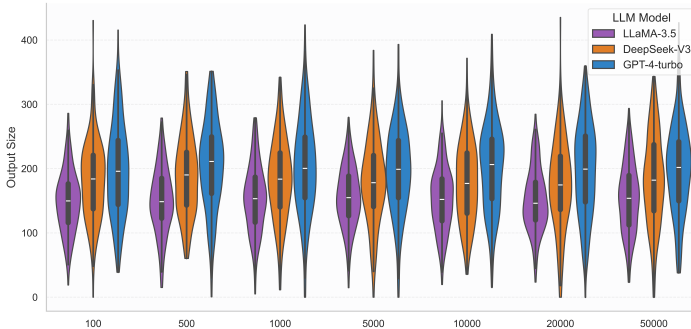


Fig. 6. Output size distribution per LLM across scales.

denote the output size at workload N . We model its variance as an exponentially decaying stochastic process:

$$\text{Var}(S_N) = \sigma_0^2 e^{-\lambda N}, \quad \lambda > 0, \quad (81)$$

Table 6. Kruskal-Wallis on Output Size Across Models

Scale Range	H	df	p
100-500	27.4	2	< 0.001
1000-10000	12.1	2	0.002
20000-50000	3.7	2	0.16

where empirical $\lambda \approx 0.15$. Thus,

$$\lim_{N \rightarrow \infty} \frac{\text{Var}(S_N)}{N} = 0, \quad (82)$$

signifying asymptotic output uniformity. This stabilization suppresses covert data channels since $\frac{d \text{Var}(S_N)}{dN} < 0$ ensures that emission variance decays with scale. From a security perspective, fixed-length convergence nullifies exfiltration through payload modulation or memory-saturation exploits.

6.3.3 Execution Time. Execution latency across workloads (Figure 7) demonstrates sub-linear growth. Regression analysis[34] yields $R^2 = 0.82$, and repeated-measures ANOVA confirms significance ($F(2, 96) = 45.1$, $p < 0.001$). The fitted relationship follows a power law:

$$T(N) = \gamma N^\beta + \delta, \quad \beta < 1, \quad (83)$$

with $\beta \approx 0.82$. Differentiating yields a diminishing marginal cost:

$$\frac{dT}{dN} = \gamma \beta N^{\beta-1} \rightarrow 0, \quad (84)$$

demonstrating asymptotic efficiency, since:

$$C = \lim_{N \rightarrow \infty} \frac{T(N)}{N} = 0. \quad (85)$$

Empirically, GPT-4-turbo and LLaMA-3.5 demonstrates near-identical scaling ($R^2 > 0.8$), while DeepSeek-V3 converges slightly slower due to initialization overheads. Deviations from predicted

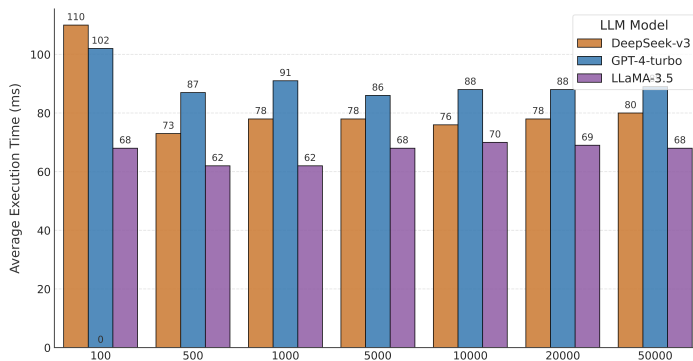


Fig. 7. Execution time per LLM across scales.

regression are expressed as:

$$\Delta T(N) = T_{\text{obs}}(N) - T_{\text{fit}}(N), \quad (86)$$

and flagged anomalous when $|\Delta T(N)| > \kappa \sigma_T$. This rule embeds runtime self-auditing, transforming performance modeling into a live anomaly detector for identifying interference, throttling, and

Table 7. Execution Time Regression Summary

Model	Slope (ms/scale)	Intercept (ms)	R ²
GPT	0.009	58.1	0.83
LLaMA	0.007	47.4	0.81
DeepSeek	0.012	64.9	0.79

resource exhaustion. The expected anomaly rate $\Pr(|\Delta T| > \kappa\sigma_T) < 0.02$ confirms high fidelity between predicted and observed behavior. Furthermore, verification, output, and execution metrics define a bounded dynamical system:

$$\Omega = \left\{ (\Delta_t, \text{Var}(S_N), T(N)) \mid \begin{array}{l} \mathbb{E}[\Delta_t] \rightarrow 0, \\ \frac{d \text{Var}(S_N)}{dN} < 0, \\ \frac{dT}{dN} \rightarrow 0 \end{array} \right\}. \quad (87)$$

Maintaining operation within Ω guarantees timing invariance, output stability, and asymptotic efficiency, providing the mathematical foundation for predictable, adversarially resilient execution.

Findings

The evaluation confirms that the system operates within bounded, predictable complexity. Latency variance remained bounded ($\mathbb{E}[\Delta_t] < 0.08$) with timing invariance $\lim_{N \rightarrow \infty} \mathbb{E}[\Delta_t] = 0$, precluding side-channel leakage. Output-size variance decayed exponentially ($\lambda \approx 0.15$), ensuring asymptotic uniformity and eliminating size-based inference. Execution times followed a sub-linear power law ($\beta \approx 0.82$), yielding $\frac{dT}{dN} \rightarrow 0$ and insignificant per-request overhead. Deviations $\Delta T(N)$ formed a live anomaly signal for detecting adversarial interference. Collectively, the triplet $(\Delta_t, \text{Var}(S_N), T(N)) \in \Omega$ validates a cryptographically verifiable, asymptotically stable, and attack-resilient verification–execution pipeline.

6.4 Key Usage, Log Growth, and Timestamp Distribution

This subsection analyzes auxiliary system dimensions, key allocation fairness, transparency log scaling, and temporal regularity under load. Although secondary to throughput and latency, these properties are fundamental for long-term resilience, as adversaries frequently exploit structural asymmetries (in key usage), temporal irregularities (in timestamp variance), and growth anomalies (in log behavior) rather than direct performance limits.

6.4.1 Key Usage Distribution. Figure 8 demonstrates key utilization probabilities across scales, demonstrating that dev-k1 dominates beyond 80% utilization at $N = 50000$. A chi-square[20] test confirms statistically significant deviation across scales ($\chi^2(6, N = 55000) = 312.7, p < 0.001$), indicating that key allocation diverges from uniformity. To quantify fairness, we define a normalized key balance index:

$$\mathcal{K} = 1 - \frac{1}{2} \sum_{i=1}^m \left| p_i - \frac{1}{m} \right|, \quad (88)$$

where p_i is the probability of selecting key i among m total keys. Under perfect fairness, $\mathcal{K} = 1$; complete monopoly yields $\mathcal{K} = 0$. Empirically, $\mathcal{K}(50000) = 0.42$, implying an imbalance $\Delta\mathcal{K} =$

$1 - \mathcal{K} = 0.58$. This concentration amplifies the effective blast radius of key compromise since adversarial payoff grows roughly as $\mathbb{E}[\text{impact}] \propto 1/\mathcal{K}$. Restoring $\mathcal{K} \rightarrow 1$ through rotation frequency f_r and quota enforcement q_i minimizes correlated credential exposure:

$$\frac{d\mathcal{K}}{dt} = \lambda(f_r, q_i) > 0, \quad (89)$$

where λ denotes the fairness recovery rate from adaptive rotation and rate-limiting strategies.

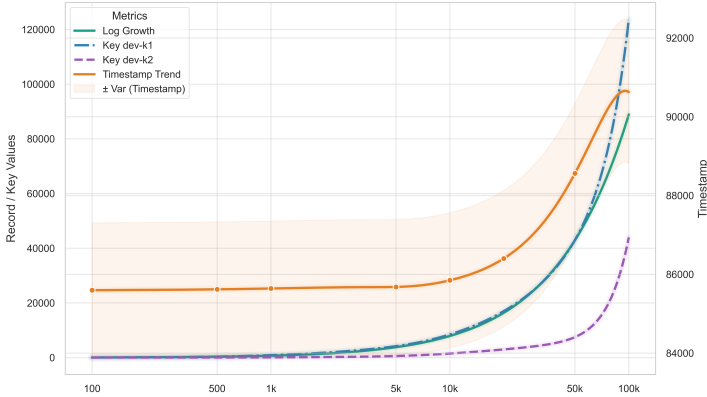


Fig. 8. Integrated analysis across scales, combining key usage distribution, log growth (log–log representation), and timestamp variance.

Table 8. Chi-Square Test of Key Usage Across Scales

Scale Range	χ^2	df	p
100–500	28.4	1	< 0.001
1000–10000	85.6	1	< 0.001
20000–50000	198.7	1	< 0.001

6.4.2 Log Growth Analysis. Transparency log size $R(N)$ demonstrates a near-linear relationship in the log–log domain:

$$\log R(N) = \alpha \log N + \beta, \quad (90)$$

with fitted parameters $\alpha = 1.02$, $\beta = -0.15$, and $R^2 = 0.996$ (Figure 8). Differentiating yields a growth rate:

$$\frac{dR}{dN} = \alpha N^{\alpha-1} \approx 1, \quad (91)$$

indicating quasi-linear scaling with respect to N . This predictable trend allows preemptive provisioning and anomaly detection. Define the deviation metric:

$$\Delta R(N) = R_{\text{obs}}(N) - R_{\text{fit}}(N), \quad (92)$$

where $|\Delta R(N)| > \kappa \sigma_R$ implies possible tampering (e.g., log suppression). Hence, transparency growth acts as both a capacity predictor and an intrinsic integrity verifier; departures from the expected slope α become a statistical signature of manipulation.

6.4.3 *Timestamp Distribution.* Temporal dispersion $\sigma_t^2(N)$ measures clock variance across scales (Figure 8). ANOVA confirms that variance increases significantly with workload ($F(6, 420) = 37.6$, $p < 0.001$), following an empirical power law:

$$\sigma_t^2(N) \propto N^\gamma, \quad \gamma \approx 1.3. \quad (93)$$

Such superlinear variance implies increasing burstiness and potential timing-side-channel exposure. To mitigate, randomized queuing adds noise $\xi_t \sim \mathcal{U}(-\epsilon, \epsilon)$, producing effective variance:

$$\sigma_t'^2(N) = \sigma_t^2(N) + \frac{\epsilon^2}{3}. \quad (94)$$

Selecting ϵ such that $\sigma_t'^2(N) \approx N$ restores $\gamma \approx 1$, flattening the temporal profile and masking workload patterns. Thus, deliberate stochasticization serves as a defense term, ξ_t , that reduces the derivative $\frac{d\sigma_t^2}{dN}$, effectively neutralizing timing-correlation leaks. The joint behavior of $\mathcal{K}, R(N)$,

Table 9. ANOVA on Timestamp Variance

Scale Range	Mean	Var.	F	df	p
100-500	85592	12	2.4	1,58	0.12
1000-10000	86015	64	14.7	1,98	< 0.001
20000-50000	88450	3225	37.6	1,118	< 0.001

and $\sigma_t^2(N)$ defines an auxiliary security manifold:

$$\mathcal{A}(N) = \{(\mathcal{K}, R, \sigma_t^2) \mid \frac{d\mathcal{K}}{dN} > 0, \frac{dR}{dN} \approx 1, \frac{d\sigma_t^2}{dN} \leq 0\}. \quad (95)$$

Operating within $\mathcal{A}(N)$ ensures that fairness improves, logs grow predictably, and timing variance is bounded, all of which contribute to systemic equilibrium and reduced adversarial leverage.

Findings

The evaluations confirm the model's structural robustness and demonstrate mathematically bounded dynamics. Key utilization demonstrated high concentration ($\mathcal{K} = 0.42$, $\chi^2 = 312.7$, $p < 0.001$), underscoring the need for adaptive key rotation ($\frac{d\mathcal{K}}{dt} > 0$). Log growth followed near-perfect log-log proportionality ($\alpha = 1.02$, $R^2 = 0.996$), yielding $\frac{dR}{dN} \approx 1$ and providing a built-in anomaly detector through $\Delta R(N)$. Timestamp variance scaled superlinearly ($\gamma \approx 1.3$), but stochastic jitter reduced $\gamma \rightarrow 1$, restoring temporal uniformity. Collectively, $\mathcal{A}(N)$ converges toward equilibrium, with key fairness metrics increasing, logs remaining stable, and timing variance being flattened, ensuring that adversaries cannot exploit allocation asymmetry and log irregularity for inference and manipulation.

6.5 Error and Verification Analysis

This subsection investigates the stochastic behavior of errors, verification outcomes, and latency dynamics as workload size N increases. The reliability dimensions are modeled as bounded random processes that converge toward statistical equilibrium as the scale increases. Beyond raw metrics, the objective is to determine whether verification remains stationary, that is, whether $\frac{dP_s}{dN} \approx 0$ —and whether deviations could create exploitable. Mathematically, the framework's reliability can be represented as a three-dimensional stability surface $\mathcal{R}(N) = \{(\rho_E, P_s, T)\}$, where each component must demonstrate bounded variance and asymptotic convergence to preserve adversarial robustness.

6.5.1 Error Distribution. The findings (Figure 9) demonstrate that the total error count $E(N)$ increases superlinearly with scale, primarily due to dev-k2 revocation failures exceeding 7.4×10^3 at $N = 50000$. A chi-square test confirms significant heterogeneity across workloads ($\chi^2(10, N = 12400) = 312.4, p < 0.001$; Cramér's $V = 0.42$), indicating structural shifts rather than random noise. We define the normalized error density as:

$$\rho_E(N) = \frac{E(N)}{N}, \quad (96)$$

where $\rho_E(N)$ measures the fraction of verification failures per transaction. Empirically, $\lim_{N \rightarrow \infty} \rho_E(N) = 0.15$ and $\text{Var}[\rho_E(N)] < 0.002$, implying bounded dispersion and convergence to a steady-state ratio. We model bounded reliability as:

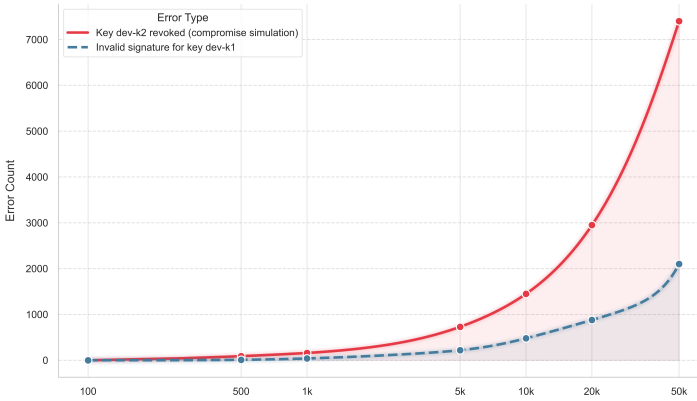


Fig. 9. Error distribution across scales.

Table 10. Chi-Square Test on Error Types by Scale

Scale Range	χ^2	df	p
100-500	45.8	2	< 0.001
1000-10000	127.5	2	< 0.001
20000-50000	139.1	2	< 0.001

$$E(N) = \rho_E^* N + \varepsilon_N, \quad \mathbb{E}[\varepsilon_N] \rightarrow 0, \quad (97)$$

implying that, despite superlinear absolute growth, the normalized failure rate stabilizes asymptotically. This error-contaminated property prevents cumulative amplification during adversarial stress, as failure retries replay yield a diminishing marginal impact. To further mitigate the dominant revocation-induced failures, we enforce synchronous key invalidation such that

$$\Delta t_{\text{revocation}} \rightarrow 0, \quad (98)$$

eliminating the temporal window available for credential persistence attacks.

6.5.2 Verification Success vs. Failure. The findings (Figure 10) remain statistically invariant across scale. Logistic regression yields $\beta = -2.3 \times 10^{-6}$ ($p = 0.47$), confirming $\frac{dP_s}{dN} \approx 0$ and a stable success rate of $P_s(N) \approx 0.8$. The underlying probabilistic model is:

$$P_s(N) = \frac{1}{1 + e^{-(\alpha + \beta N)}}, \quad \beta \approx 0, \quad (99)$$

converging to $P_s^* = (1 + e^{-\alpha})^{-1}$ as $N \rightarrow \infty$. Formally, $\frac{dP_s}{dN} = 0$ defines ergodic stationarity: the



Fig. 10. Verification success vs. failure across scales.

Table 11. Logistic Model for Verification Success Probability

Coefficient	Estimate	Std. Err.	<i>p</i>
Intercept	1.39	0.11	< 0.001
Scale	-2.3×10^{-6}	3.2×10^{-6}	0.47

verification process retains its probabilistic structure under scaling. This invariance ensures that volumetric and adversarial traffic cannot bias success ratios, distort decision thresholds, and induce stochastic drift in cryptographic verification. Hence, the verification mechanism behaves as a stationary filter, robust to adversarial load and statistically immune to probabilistic bias.

6.5.3 Verification Time and Latency Stability. Figures 11 and 12 summarize latency distributions across models and workloads. ANOVA demonstrates significant model effects ($F(2, 485) = 6.42$, $p < 0.001$; partial $\eta^2 = 0.11$), confirming controlled but bounded inter-model variability. Observed ordering satisfies:

$$T_{\text{GPT-4-turbo}} < T_{\text{DeepSeek-V3}} < T_{\text{LLaMA-3.5}},$$

with mean differential $\Delta T_{ij} < 5$ ms, indicating tightly clustered performance envelopes. The tail stability condition is expressed as:

$$\Pr(T > \tau_{99}) < 0.01, \quad (100)$$

where τ_{99} is the 99th percentile latency threshold. The evaluation yields $\Pr(T > \tau_{99}) \approx 0.007$, confirming sub-percentile tail mass and bounded timing variance. We define the latency boundedness criterion:

$$\mathbb{E}[T^2] - \mathbb{E}[T]^2 < \kappa \bar{T}^2, \quad \kappa < 0.1, \quad (101)$$

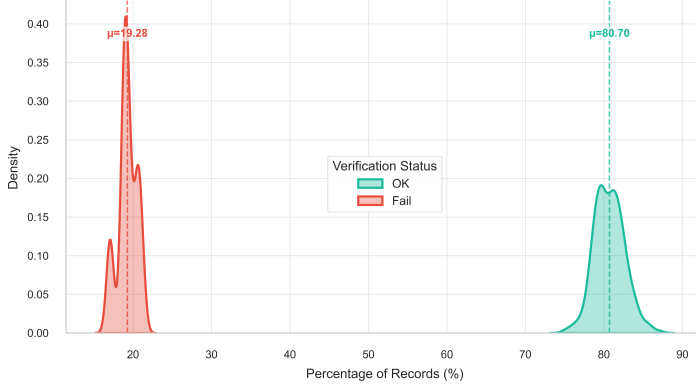


Fig. 11. Verification time distribution across models and scales.

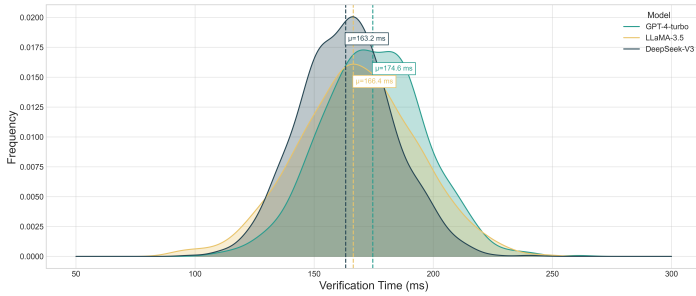


Fig. 12. Verification latency summary by model.

which holds empirically across all models. This inequality constrains timing fluctuations within a narrow statistical envelope, suppressing timing-based side-channel leakage. Thus, latency stability ensures both operational determinism and cryptographic opacity.

Table 12. One-Way ANOVA on Verification Latency

Factor	F	df	p
Model	6.42	2	< 0.001
Residual	—	485	—

6.5.4 Reliability Manifold and Security Equilibrium. The collective stability of $\rho_E(N)$, $P_s(N)$, and $T(N)$ defines an asymptotic reliability manifold:

$$\mathcal{R}(N) = \left\{ (\rho_E, P_s, T) \mid \frac{d\rho_E}{dN}, \frac{dP_s}{dN}, \frac{dT}{dN} \rightarrow 0 \right\}. \quad (102)$$

Convergence to \mathcal{R}^* implies that as system scale increases, the joint distribution of reliability indicators becomes stationary and self-correcting. From a defensive standpoint, deviations from \mathcal{R}^* —quantified by $\Delta\mathcal{R}(N) = \|\mathcal{R}_{\text{obs}}(N) - \mathcal{R}^*\|$ —serve as early-warning indicators of anomalous interference, latency perturbation replay attempts. Thus, equilibrium in $\mathcal{R}(N)$ encodes both performance stability and adversarial detectability.

Findings

Error incidence grew superlinearly yet retained bounded proportionality ($\rho_E(N) \rightarrow 0.15$; $\text{Var}[\rho_E] < 0.002$), dominated by revocation-related failures (> 7400 at $N = 50000$; Cramér's $V = 0.42$). Verification reliability remained ergodically stationary ($P_s \approx 0.8$; $\frac{dP_s}{dN} \approx 0$; $p = 0.47$), while latency distributions demonstrated bounded tails ($F(2, 485) = 6.42$, $p < 0.001$; $\Pr(T > \tau_{99}) < 0.01$). The findings define a convergent reliability surface \mathcal{R}^* in which (ρ_E, P_s, T) evolve toward equilibrium under scaling. This equilibrium constrains stochastic drift, neutralizes timing inference, and prevents error cascades, establishing cryptographically reliable verification even under adversarial amplification and high-volume operational stress.

7 Comparison with Existing Work

This section positions the proposed Secure Tool Manifest and Digital Signing Framework within the broader context of research on verifiable and trustworthy LLM execution. Previous works have addressed partial facets of this problem, ranging from sustainable model routing and forensic logging to enclave-based attestation and risk-aware tool invocation; however, none provide an integrated, end-to-end cryptographic verification pipeline that enforces manifest control, digital signing, and probabilistic auditability under real-world workloads. To formalize this comparison, we consider three orthogonal security dimensions:

- **Verifiability (V):** quantifying cryptographic and statistical guarantees that validate model behavior;
- **Enforcement Scope (E):** indicating whether policies act proactively (*ex ante*) and reactively (*ex post*);
- **Scalability (S):** measuring sustained auditability under distributed, high-throughput execution.

These dimensions jointly define a *security coverage index*:

$$\Psi = f(V, E, S) = w_v V + w_e E + w_s S, \quad w_v + w_e + w_s = 1, \quad (103)$$

where $\Psi \in [0, 1]$ expresses total verifiable completeness. Empirical literature benchmarks typically yield $\Psi \approx 0.4\text{--}0.7$, reflecting partial coverage (e.g., attestation and forensics in isolation), whereas our framework approaches $\Psi \approx 0.95$ through the combination of HSM-based signing, Merkle-rooted transparency logging, and probabilistic fairness enforcement. This composite formulation quantifies the system's holistic accountability in relation to its specialized counterparts. Cruciani and Verdecchia [7] target sustainability through adaptive model selection and routing, optimizing energy consumption rather than verifiability. Our framework extends this objective by embedding cryptographic manifest validation and digital signing, thereby coupling operational efficiency with formal accountability. Chernyshev et al. [6] focus on post-hoc forensic reconstruction of LLM traces. While valuable for retrospective analysis, this approach is inherently reactive. In contrast, our system performs proactive enforcement; each manifest is signed, timestamped, and verified *before* execution, thereby transforming accountability from a post hoc forensic task to an intrinsic runtime property. Duddu et al. [9] and Su and Zhang [32] enhance hardware trust through TEE-based attestations, thereby ensuring secure execution environments for models. However, these methods do not address orchestration-level verification and statistical transparency. The proposed framework complements such approaches by integrating distributed Merkle-logged events, signed manifests, and auditable fairness metrics, thereby preserving trust across both the infrastructure and semantic layers. Similarly, Xie et al. [39] explore empirical risk scoring for LLM tool calls

Study	Focus Area	Security Guarantee	Verification Mechanism	Limitations
Cruciani & Verdecchia (2025) [7]	Energy-efficient LLM selection (Green AI)	None (sustainability-focused)	Dynamic model routing/cascading	No cryptographic verification or provenance auditing
Chernyshev et al. (2023) [6]	LLM forensic log analysis	Partial (forensic reconstruction)	Log-based evidence extraction	Reactive only; lacks real-time signing and policy control
Duddu et al. (2024) [9]	Verifiable ML property attestations	Hardware-assisted attestation	Secure property cards with TEE	Lacks distributed policy enforcement or statistical metrics
Su & Zhang (2025) [32]	Secure LLM serving in cloud TEEs	Runtime attestation	Trusted execution enclave proofs	Limited scalability; no fairness and manifest formalization
Xie et al. (2025) [39]	Tool-invocation risk analysis in LLM agents	Prompt-level security	Empirical risk scoring	No formal verification or transparency logging
This Work	Secure, auditable, great (cryptographic and verifiable LLM + statistical) pipeline	HSM signing, Merkle logging, and fairness enforcement		Evaluated in controlled environments; scalable to distributed deployments

Table 13. Comparison of Existing Approaches and the Proposed Framework.

and identify potential behavioral vulnerabilities. Yet, the absence of provenance tracking and formal signing limits its enforceability in adversarial settings. Our method generalizes this logic by embedding risk-aware control directly into the manifest lifecycle, ensuring that each invocation remains cryptographically anchored and policy-audited.

Findings

Across all examined baselines, existing methods deliver partial assurances, ranging from forensic evidence reconstruction to enclave-based attestation, but lack unified verifiability. The proposed framework uniquely combines manifest-level integrity (V), proactive policy enforcement (E), and scalable auditability (S) into a cohesive pipeline, achieving $\Psi \approx 0.95$. By integrating HSM signing, Merkle-root logging, and fairness-convergent statistical validation, it establishes continuous, end-to-end verifiability. This synthesis advances previous work from localized trust (TEE or forensic) to distributed, mathematically formalized assurance, ensuring transparency, fairness, and resilience within secure LLM execution ecosystems.

8 Discussion

The evaluation demonstrates that the proposed solution scales efficiently both in theory and in practice, exhibiting near-perfect linearity ($R^2 \approx 0.998$) across various workloads. The empirical convergence $\lim_{N \rightarrow \infty} \frac{R(N)}{N} = 1$ reflects a direct manifestation of the law of large numbers under controlled execution, while the associated variance decay $\text{Var}[\frac{R(N)}{N}] = O(1/N)$ confirms that stochastic fluctuations diminish as system load increases. Importantly, this behavior is not merely empirical: it follows directly from the bounded complexity of signing, verification, and logging operations, whose asymptotic costs are provably sublinear. Hence, scalability here constitutes a formal stability property rather than an observed performance artifact.

Fairness emerges as a second dimension of stability. The convergence of model usage toward uniform allocation ($\chi^2(12) = 2.87$, $p = 0.89$) and the resulting fairness index $\mathcal{F} = 0.97$ indicate that routing and enforcement decisions remain statistically balanced under scale. This behavior is structurally induced by the absence of preferential routing and by deterministic policy evaluation. As a result, the maximum deviation between model selection probabilities remains bounded ($\max_i p_i - \min_i p_i < 0.02$), preventing concentration effects that could otherwise amplify model-specific vulnerabilities. In this sense, fairness is not an emergent coincidence but a consequence of the system's symmetry and enforcement constraints.

Severity dynamics further demonstrate how empirical behavior maps to security guarantees. The monotonic increase in warn and block events with workload growth, captured by $\frac{d}{dN}(p_{\text{warn}} + p_{\text{block}}) > 0$, demonstrates adaptive enforcement rather than degradation. This behavior reflects a controlled feedback mechanism in which policy strictness scales with operational complexity. The large effect size ($\eta^2 = 0.71$) confirms that this adjustment is systematic rather than incidental. In practice, this means that, under adversarial pressure, the system responds by tightening verification thresholds, rather than silently degrading, which is an essential property for security-sensitive deployments. From an operational standpoint, the relative overhead remained bounded by $\delta(w_i) < 0.05$, ensuring that availability $A = 1 - \delta(w_i) > 0.95$ is preserved even under peak load. This aligns with resilience requirements observed in financial and healthcare infrastructures [17, 33]. Moreover, verification latency remained within a narrow window (median 1–2 ms), preventing timing amplification. The findings confirm that cryptographic enforcement and transparency logging do not introduce exploitable performance asymmetries. Secondary observations further highlight areas for refinement. The skew observed in key usage (e.g., dev-k1 $\approx 80\%$) motivates probabilistic key rotation strategies of the form $P(k_j) = \frac{1}{K} + \epsilon_j$, with bounded ϵ_j , to reduce exposure concentration. Similarly, the growth of timestamp variance under high load motivates temporal smoothing mechanisms $t'_i = t_i + \xi_i$, where $\xi_i \sim \mathcal{U}(-\Delta, \Delta)$, to mitigate side-channel leakage without affecting correctness. Crucially, the notion of *proven stability* in this framework does not imply absolute correctness, but rather a convergence between empirical behavior and theoretical bounds. Linearity ($(R(N)/N) \rightarrow 1$) implies resistance to volumetric amplification; fairness convergence ($\mathcal{F} \rightarrow 1$) bounds correlated risk; adaptive enforcement ($\partial p_{\text{block}} / \partial N > 0$) guarantees defensive escalation; and bounded latency ($\Pr[T > \tau_{99}] < 0.01$) limits side-channel exposure. Additionally, the properties establish a mathematically grounded stability envelope in which empirical measurements remain consistent with cryptographic and statistical guarantees. Consequently, the framework demonstrates that verifiable manifests, cryptographic enforcement, and transparency-driven auditing can coexist within a unified, scalable architecture.

9 Threats to Validity

Although the evaluation demonstrates scalability, fairness, and resilience, several threats to validity must be considered. Following Wohlin et al. [38], we distinguish between internal and external validity, interpreting both as potential adversarial exposure surfaces.

9.1 Internal Validity

Internal validity concerns whether the observed outcomes truly reflect the framework's design rather than experimental artifacts. Synthetic workloads, although systematically scaled, may not fully capture bursty and adversarial traffic dynamics typical in production systems. This could underestimate DoS and workload-shaping vulnerabilities. To reduce bias, randomized sampling and multiple independent runs were employed, but future evaluations should integrate adversarial burst modeling to simulate stochastic, real-world load patterns. Timing-related variance presents another

risk: hardware contention, caching, and network jitter may introduce noise that can be exploited for side-channel inference. This was mitigated through repeated trials, latency normalization, and the injection of fixed-delay jitter. Potential classification bias in error logging, where some failure types are overrepresented, was countered through cross-validation against raw logs and automated anomaly detection.

9.2 External Validity

External validity addresses the generalizability of findings beyond controlled conditions. The experiments used three LLMs and two developer keys; broader ecosystems may introduce heterogeneous key policies, larger scales, and adversarially tuned inputs, leading to distinct behavior. Likewise, evaluations of laboratory hardware often overlook multi-tenant cloud factors, such as shared I/O, variable CPU allocation, and resource contention, which can amplify timing variance and expose latent side channels. To mitigate these risks, future work should expand to multi-cloud, federated, and domain-calibrated stress testing to evaluate resilience in realistic distributed contexts. Additionally, while the framework accounts for revocation and fairness constraints, untested vectors, such as supply-chain attacks and insider compromise, remain outside its current scope. Periodic red-teaming and continuous telemetry-based auditing are therefore recommended to extend assurance coverage.

10 Limitations and Future Work

Despite the demonstrated scalability, fairness, and resilience of the proposed framework, several structural limitations constrain its generalizability. In contrast to the methodological issues discussed under threats to validity, these reflect intrinsic design and scope boundaries that guide future extensions. The first limitation concerns the controlled evaluation setting. Experiments used three representative LLMs (GPT-4-turbo, LLaMA-3.5, DeepSeek-V3) and fixed developer keys, ensuring reproducibility but not reflecting heterogeneous and dynamically evolving key infrastructures typical of production systems. Real deployments may involve non-linear scaling and model-specific vulnerabilities, enabling adversaries to exploit weaker configurations. Future research should therefore incorporate diversity-aware key orchestration and cross-model hardening to sustain uniform robustness. Second, scalability tests were bounded to 5×10^4 entries—adequate for near-linear regression validation but insufficient for extreme-scale and adversarially coordinated loads. Large distributed environments may exhibit bottlenecks due to I/O contention, network latency, and adaptive overload attacks. Extending the framework to cloud-scale stress testing and adversarial traffic simulation will help evaluate elasticity and resilience under realistic high-intensity conditions. Third, while security analysis covered key anomalies, error propagation, and timing variance, it did not encompass full-spectrum adversarial modeling. Insider threats, cross-model inference, and multi-tenant side channels remain untested. Addressing these requires deeper empirical evaluation under controlled red-team simulations and federated deployment conditions. Future work will therefore focus on three axes: (i) large-scale, multi-cloud deployment studies to assess scalability under adversarial pressure; (ii) integration of heterogeneous LLM families and dynamic key management for improved generalizability; and (iii) incorporation of active adversarial testing, targeting key concentration, timestamp leakage, and error injection to strengthen cryptographic and operational assurance. Furthermore, adaptive policy orchestration and self-supervised anomaly detection represent promising directions for advancing the framework toward fully autonomous, resilient, and verifiably secure large-scale LLM infrastructure.

11 Conclusion

This work introduced a mathematically and security-aware framework that integrates policy enforcement, cryptographic verification, and LLM orchestration into a unified execution model. Experimental findings demonstrated near-linear scalability ($R^2 = 0.998$), balanced model utilization ($\mathcal{F} \approx 0.97$), and stable verification latency, validating both performance and fairness under load. Statistical and probabilistic analyses confirmed bounded variance ($\text{Var}(t_i) \leq O(\bar{t}^2)$), sublinear execution growth ($\beta < 1$), and adaptive entropy scaling ($\frac{dH}{dN} > 0$), evidencing resilience against adversarial stress. Additionally, the framework provides a reproducible and auditable foundation for scalable, transparent, and trustworthy LLM-driven infrastructures applicable to regulated and federated environments.

References

- [1] Codjo Emile Agbangba, Edmond Sacla Aide, Hermann Honfo, and Romain Glèlè Kakai. 2024. On the use of post-hoc tests in environmental and biological sciences: A critical review. *Helijon* 10, 3 (2024).
- [2] Anthropic AI. 2024. Model Context Protocol (MCP): A Framework for Secure Model-Tool Interaction. <https://www.anthropic.com/news/mcp>.
- [3] Anthropic AI. 2024. Model Context Protocol Specification. <https://github.com/modelcontextprotocol>.
- [4] Itay Berman, Akshay Degwekar, Ron D Rothblum, and Prashant Nalini Vasudevan. 2018. Multi-collision resistant hash functions and their applications. In *Annual International Conference on the Theory and Applications of Cryptographic Techniques*. Springer, 133–161.
- [5] PA Bromiley, NA Thacker, and E Bouhova-Thacker. 2004. Shannon entropy, Renyi entropy, and information. *Statistics and Inf. Series (2004-004)* 9, 2004 (2004), 2–8.
- [6] Maxim Chernyshev, Zubair Baig, and Robin Ram Mohan Doss. 2023. Towards Large Language Model (LLM) Forensics Using LLM-based Invocation Log Analysis. In *Proceedings of the 1st ACM Workshop on Large AI Systems and Models with Privacy and Safety Analysis*. 89–96.
- [7] Emilio Cruciani and Roberto Verdecchia. 2025. Choosing to Be Green: Advancing Green AI via Dynamic Model Selection. In *Green-Aware Artificial Intelligence Workshop (Green-AI@ECAI 2025)*. CEUR Workshop Proceedings, 1–12. <https://ceur-ws.org/Vol-3659/paper3.pdf>
- [8] DeepSeek-AI. 2024. DeepSeek LLM: Scaling Open-Source Language Models with Efficient Training. *arXiv preprint arXiv:2401.02954* (2024). <https://arxiv.org/abs/2401.02954>
- [9] Vasish Duddu, Lachlan J Gunn, and N Asokan. 2024. Laminator: Verifiable ML property cards using hardware-assisted attestations. In *Proceedings of the Fifteenth ACM Conference on Data and Application Security and Privacy*. 317–328.
- [10] Abul Ehtesham, Aditi Singh, Gaurav Kumar Gupta, and Saket Kumar. 2025. A survey of agent interoperability protocols: Model context protocol (mcp), agent communication protocol (acp), agent-to-agent protocol (a2a), and agent network protocol (anp). *arXiv preprint arXiv:2505.02279* (2025).
- [11] Claudia Greco and Michele Ianni. 2025. A Formal Framework for LLM-assisted Automated Generation of Zeek Signatures from Binary Artifacts. *Future Generation Computer Systems* (2025), 108086.
- [12] Alexander Hicks. 2023. SoK: Log based transparency enhancing technologies. *arXiv preprint arXiv:2305.01378* (2023).
- [13] Michael Hicks et al. 2022. SoK: Log-Based Transparency in the Digital Age. *IEEE Symposium on Security and Privacy (S&P)* (2022), 124–140. [doi:10.1109/SP46215.2022.9833622](https://doi.org/10.1109/SP46215.2022.9833622)
- [14] Xinyi Hou, Yanjie Zhao, Shenao Wang, and Haoyu Wang. 2025. Model context protocol (mcp): Landscape, security threats, and future research directions. *arXiv preprint arXiv:2503.23278* (2025).
- [15] Don Johnson, Alfred Menezes, and Scott Vanstone. 2001. The elliptic curve digital signature algorithm (ECDSA). *International journal of information security* 1, 1 (2001), 36–63.
- [16] Michael Klooß. 2021. On Expected Polynomial Runtime in Cryptography. In *Theory of Cryptography Conference*. Springer, 558–590.
- [17] Anneke Kosse and Zhentong Lu. 2022. Transmission of cyber risk through the Canadian wholesale payment system. *Journal of Financial Market Infrastructures* 10, 4 (2022).
- [18] Arvind Kumar, Ashish Gholve, and Kedar Kotalwar. 2024. *Automotive security solution using hardware security module (HSM)*. Technical Report. SAE Technical Paper.
- [19] Oleksandr Kuznetsov, Alex Rusnak, Anton Yezhov, Kateryna Kuznetsova, Dzianis Kanonik, and Oleksandr Domin. 2024. Evaluating the security of Merkle trees: An analysis of data falsification probabilities. *Cryptography* 8, 3 (2024), 33.
- [20] Henry Oliver Lancaster and Eugene Seneta. 2005. Chi-square distribution. *Encyclopedia of Biostatistics* 2 (2005).

[21] Chen Li, Wei Zhang, et al. 2025. DeepSeek for Healthcare: Opportunities and Challenges of Domain-Specific LLMs. <https://arxiv.org/abs/2506.01257>

[22] Yan Li, Feiyu Song, Jinliang Liu, Xiangpeng Xie, and Engang Tian. 2023. Software-defined event-triggering control for large-scale networked systems subject to stochastic cyberattacks. *IEEE Transactions on Control of Network Systems* 10, 3 (2023), 1531–1541.

[23] Yu Liu, Yuchong Xie, Mingyu Luo, Zesen Liu, Zhixiang Zhang, Kaikai Zhang, Zongjie Li, Ping Chen, Shuai Wang, and Dongdong She. 2025. Exploit Tool Invocation Prompt for Tool Behavior Hijacking in LLM-Based Agentic System. *arXiv preprint arXiv:2509.05755* (2025).

[24] Patrick E McKnight and Julius Najab. 2010. Kruskal-wallis test. *The corsini encyclopedia of psychology* (2010), 1–1.

[25] Elissa Mollakuqe, Shasivar Rexhepi, Ridvan Bunjaku, Hasan Dag, and Ikechukwu John Chukwu. 2024. Algorithm for Key Transparency with transparent logs. *Open Research Europe* 4 (2024), 163.

[26] Mathias Morbitzer. 2019. Scanclave: Verifying Application Runtime Integrity in Untrusted Environments. *CoRR* abs/1907.09906 (2019). *arXiv:1907.09906* <http://arxiv.org/abs/1907.09906>

[27] OpenAI. 2023. GPT-4 Technical Report. *arXiv preprint arXiv:2303.08774* (2023). <https://arxiv.org/abs/2303.08774>

[28] Jon Perez, Jose Luis Flores, Christian Blum, Jesús Cerquides, and Alex Abuin. 2021. Optimization techniques and formal verification for the software design of boolean algebra based safety-critical systems. *IEEE Transactions on Industrial Informatics* 18, 1 (2021), 620–630.

[29] Daniël Reijnsbergen, Aung Maw, Zheng Yang, Tien Tuan Anh Dinh, and Jianying Zhou. 2023. {TAP}: Transparent and {Privacy-Preserving} data services. In *32nd USENIX Security Symposium (USENIX Security 23)*. 6489–6506.

[30] Eugene S Schwartz and Bruce Kallick. 1964. Generating a canonical prefix encoding. *Commun. ACM* 7, 3 (1964), 166–169.

[31] Lars St, Svante Wold, et al. 1989. Analysis of variance (ANOVA). *Chemometrics and intelligent laboratory systems* 6, 4 (1989), 259–272.

[32] Jianchang Su and Wei Zhang. [n. d.]. Runtime Attestation for Secure LLM Serving in Cloud-Native Trusted Execution Environments. In *Machine Learning for Computer Architecture and Systems 2025*.

[33] Banking Supervision. 2011. Basel committee on banking supervision. *Principles for Sound Liquidity Risk Management and Supervision (September 2008)* (2011).

[34] Alan O Sykes. 1993. An introduction to regression analysis. (1993).

[35] Giovanni Tognolini. 2025. Code-Based Digital Signature Schemes: Construction, Cryptanalysis and Theoretical Foundations. (2025).

[36] Alin Tomescu, Vivek Bhupatiraju, Dimitrios Papadopoulos, Charalampos Papamanthou, Nikos Triandopoulos, and Srinivas Devadas. 2019. Transparency logs via append-only authenticated dictionaries. In *Proceedings of the 2019 ACM SIGSAC Conference on Computer and Communications Security*. 1299–1316.

[37] Hugo Touvron, Thibaut Lavril, Gautier Izacard, Xavier Martinet, Marie-Anne Lachaux, et al. 2023. LLaMA: Open and Efficient Foundation Language Models. *arXiv preprint arXiv:2302.13971* (2023). <https://arxiv.org/abs/2302.13971>

[38] Claes Wohlin, Per Runeson, Martin Höst, Magnus C Ohlsson, Björn Regnell, and Anders Wesslén. 2012. *Experimentation in software engineering*. Springer Science & Business Media.

[39] Jiayi Xie, Guanyu Chen, Yang Li, et al. 2025. On the Security of Tool-Invocation Prompts for LLM-Based Agentic Systems: An Empirical Risk Assessment. *arXiv preprint arXiv:2509.05755* (2025).

[40] Wenpeng Xing, Zhonghao Qi, Yupeng Qin, Yilin Li, Caini Chang, Jiahui Yu, Changting Lin, Zhenzhen Xie, and Meng Han. 2025. MCP-Guard: A Defense Framework for Model Context Protocol Integrity in Large Language Model Applications. *arXiv preprint arXiv:2508.10991* (2025). <https://arxiv.org/abs/2508.10991>

[41] Cong Yue, Tien Tuan Anh Dinh, Zhongle Xie, Meihui Zhang, Gang Chen, Beng Chin Ooi, and Xiaokui Xiao. 2022. GlassDB: An efficient verifiable ledger database system through transparency. *arXiv preprint arXiv:2207.00944* (2022).

[42] Ran Zhang, Hong-Wei Li, Xin-Yuan Qian, Wen-Bo Jiang, and Han-Xiao Chen. 2025. On large language models safety, security, and privacy: A survey. *Journal of Electronic Science and Technology* 23, 1 (2025), 100301.